# The Equatorial Energy Balance, ITCZ Position, and Double-ITCZ Bifurcations

TOBIAS BISCHOFF

*California Institute of Technology, Pasadena, California*

TAPIO SCHNEIDER

*ETH Zurich, Zurich, Switzerland, and California Institute of Technology, Pasadena, California*

(Manuscript received 6 May 2015, in final form 3 August 2015)

ABSTRACT

The intertropical convergence zone (ITCZ) migrates north–south on seasonal and longer time scales. Previous studies have shown that the zonal-mean ITCZ displacement off the equator is negatively correlated with the energy flux across the equator; when the ITCZ lies in the Northern Hemisphere, energy flows southward across the equator, and vice versa. The hemisphere that exports energy across the equator is the hemisphere with more net energy input, and it is usually the warmer hemisphere. But states with a double ITCZ straddling the equator also occur, for example, seasonally over the eastern Pacific and frequently in climate models. Here it is shown how the ITCZ position is connected to the energy balance near the equator in a broad range of circumstances, including states with single and double ITCZs. Taylor expansion of the variation of the meridional energy flux around the equator leads to the conclusion that for large positive net energy input into the equatorial atmosphere, the ITCZ position depends linearly on the cross-equatorial energy flux. For small positive equatorial net energy input, the dependence of the ITCZ position on the cross-equatorial energy flux weakens to the third root. When the equatorial net energy input or its curvature become negative, a bifurcation to double-ITCZ states occurs. Simulations with an idealized aquaplanet general circulation model (GCM) confirm the quantitative adequacy of these relations. The results provide a framework for assessing and understanding causes of common climate model biases and for interpreting tropical precipitation changes, such as those evident in records of climates of the past.

## 1. Introduction

The bulk of the tropical precipitation falls in the intertropical convergence zone (ITCZ), a band of convective clouds in the tropics that migrates meridionally on seasonal and longer time scales. In the zonal mean, precipitation has one maximum that migrates from the Northern Hemisphere tropics in boreal summer to the Southern Hemisphere tropics in boreal winter. Locally, however, the precipitation can have more than one maximum in a given sector of longitudes. For example, over the eastern Pacific, the ITCZ is located north of the equator most of the year, meandering by a few degrees latitude around 6°. However, for a brief period in spring (Zhang 2001; Xie and Yang 2014), it splits into two ITCZs straddling the equator (Fig. 1a). Current climate models exaggerate this split into two ITCZs (Fig. 1b), leading to the well-known double-ITCZ bias of the models (e.g., Lin 2007; Hwang and Frierson 2013).

Many previous studies, analyzing observations and simulations, have shown that the position of the ITCZ is negatively correlated with the strength of the zonal-mean energy flux across the equator (e.g., Broccoli et al. 2006; Yoshimori and Broccoli 2008; Kang et al. 2008, 2009; Frierson and Hwang 2012; Donohoe et al. 2013). Because the energy flux across the equator is generally directed from the warmer into the cooler hemisphere and strengthens with the temperature contrast between the hemispheres (Bischoff and Schneider 2014), the ITCZ position is also correlated with the interhemispheric temperature contrast (e.g., Chiang and Bitz 2005; Chiang and Friedman 2012; Cvijanovic and Chiang 2013; Friedman et al. 2013). Despite this progress,

*Corresponding author address*: Tobias Bischoff, Division of Geological and Planetary Sciences, 1200 E California Blvd., Pasadena, CA 91125.
E-mail: tobias@caltech.edu

DOI: 10.1175/JCLI-D-15-0328.1

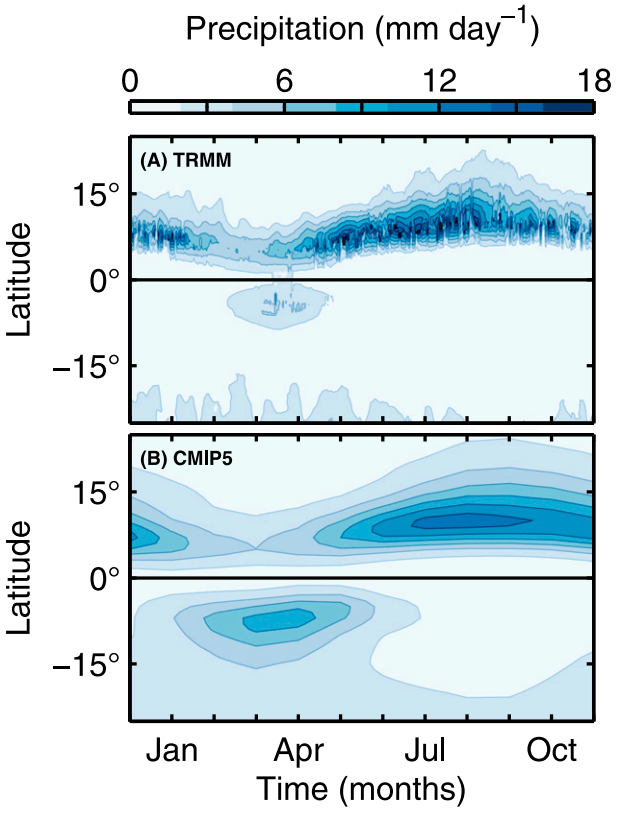


FIG. 1. Annual cycle of eastern Pacific precipitation in observations and climate simulations. (a) Observed daily precipitation rates from the Tropical Rainfall Measuring Mission (TRMM) Multisatellite Precipitation Analysis (TMPA; Liu et al. 2012), averaged over the years 1998–2012. (b) Simulated monthly precipitation rates from the ensemble mean of CMIP5 models, including all models for which these data are available. (For models for which multiple runs were available, only the first one is included.) In both panels, the precipitation rates are averaged over the longitude sector between 100° and 140°W. During spring in the eastern Pacific, the ITCZ splits into two ITCZs north and south of the equator in observations and simulations. However, climate models exaggerate this split in duration and intensity.

however, it has remained unclear how the ITCZ position is generally related to the atmospheric energy balance. We have recently shown that if the meridional energy flux varies approximately linearly with latitude around the equator, the ITCZ position is proportional to the strength of the cross-equatorial energy flux and inversely proportional to the flux divergence at the equator, or the equatorial net energy input (Bischoff and Schneider 2014; Schneider et al. 2014). Here we expand on that work to show how the ITCZ position relates to the energy balance near the equator more generally, even when the energy flux varies nonlinearly with latitude around the equator. This provides a framework within which bifurcations to double-ITCZ states, such as those occurring seasonally over the Pacific or frequently in climate models, can also be understood and analyzed.

As in Bischoff and Schneider (2014), we test the theoretical developments to be presented with simulations with an idealized aquaplanet GCM. This affords tests over a very broad range of simulated climates, with continuous variations of ITCZ positions and bifurcations from single to double ITCZs. Section 2 provides an overview of the idealized GCM used in this study and introduces the different forcing scenarios with which we generate a wide range of different ITCZs. Section 3 describes how the ITCZ position relates to mass and energy fluxes. Section 4 discusses how the ITCZ position is linked to the equatorial energy balance and specifically to the meridional energy flux and its derivatives at the equator. The theoretical developments are illustrated and tested with the idealized GCM simulations. Section 5 summarizes our results and discusses some of their implications for climate modeling and the interpretation of climate records. The appendix contains theoretical considerations that supplement those in section 4.

## 2. Idealized GCM simulations

### a. Model

The idealized GCM used in this study integrates the hydrostatic primitive equations using the spectral dynamical core of the Geophysical Fluid Dynamics Laboratory's flexible modeling system. It uses T85 spectral resolution in the horizontal and, in the vertical, 30 unevenly spaced $\sigma$ levels, where $\sigma = p/p_s$, with $p$ denoting pressure and $p_s$ surface pressure. The GCM is similar to the one described in Frierson (2007), O'Gorman and Schneider (2008), or Merlis et al. (2013). It employs a two-stream gray radiation scheme, with shortwave and longwave absorption in the atmosphere modeled using time-independent zonally symmetric absorber profiles. Atmospheric scattering of radiation is not explicitly taken into account; the effect of shortwave scattering on the surface energy balance is taken into account by using an enhanced surface albedo (O'Gorman and Schneider 2008).

The GCM has a simple representation of the hydrological cycle, modeling only the vapor–liquid phase transition with a fixed latent heat of vaporization $L_v = 2.6 \times 10^6\ \mathrm{J\,kg^{-1}}$. Water vapor condenses when saturation is reached at the grid scale. Additionally, the model also uses a quasi-equilibrium convection scheme that relaxes convectively unstable atmospheric columns to a moist-pseudoadiabatic temperature profile with a fixed relative humidity of 70% (Frierson 2007; O'Gorman and Schneider 2008). Reevaporation of precipitation is not taken into account, and precipitation from convection and grid-scale condensation is returned to the surface instantly.

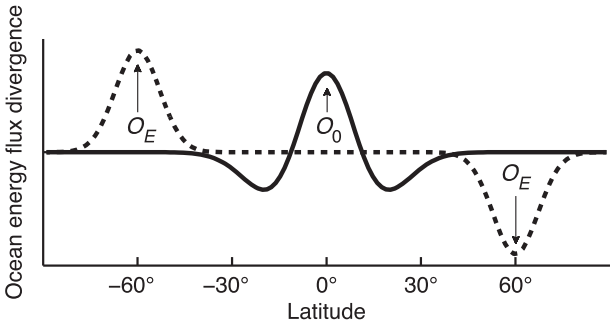


FIG. 2. Sketch of the imposed ocean energy flux divergence in the idealized GCM simulations. The two parameters varied are $O_0$, the amplitude of the equatorial ocean energy flux divergence, and $O_E$, the amplitude of the extratropical ocean energy flux divergence. The solid line shows the symmetric component of the ocean energy flux divergence, and the dashed line shows the antisymmetric component. Both are varied independently of each other from 0 to 100 W m$^{-2}$ in steps of 10 W m$^{-2}$, resulting in a total of 121 simulations.

The lower boundary is modeled as a slab ocean surface with a constant uniform albedo of $\alpha = 0.3$, satisfying the surface energy balance:

$$\rho c_0 d \partial_t T_{\mathrm{sfc}} = \mathcal{S}_{\mathrm{sfc}} - \mathcal{L}_{\mathrm{sfc}} - \mathcal{E} - \mathcal{H} - \mathcal{O}, \tag{1}$$

where the constants $\rho = 1000\,\mathrm{kg\,m^{-3}}$ denote the surface water density, $c_0 = 4000\,\mathrm{J\,kg^{-1}\,K^{-1}}$ the surface water heat capacity, $d = 1\,\mathrm{m}$ the depth of the ocean slab (coarsely representing the mixed layer); the variable $T_{\mathrm{sfc}}$ denotes the surface temperature, $\mathcal{S}_{\mathrm{sfc}}$ the net downwelling shortwave radiation at the surface, $\mathcal{L}_{\mathrm{sfc}}$ the net upwelling longwave radiation at the surface, $\mathcal{E}$ the latent heat flux associated with surface evaporation, and $\mathcal{H}$ the sensible heat flux. The fluxes $\mathcal{E}$ and $\mathcal{H}$ are represented via standard bulk aerodynamic formulas.

The term $\mathcal{O}$ in the surface energy balance in (1) represents ocean energy flux divergence and is the primary quantity we vary to generate different ITCZ structures. The ocean energy flux divergence is prescribed to be time independent and zonally symmetric, of the following form (see Fig. 2):

$$\mathcal{O} = O_0 \cos(\phi)^{-1} \left(1 - \frac{\phi^2}{\delta\phi_0^2}\right) \exp\left[-\frac{\phi^2}{2\delta\phi_0^2}\right] \tag{2a}$$

$$+ O_E \exp\left[-\frac{(\phi + \phi_{\mathrm{NH}})^2}{2\delta\phi_E^2}\right] \tag{2b}$$

$$- O_E \exp\left[-\frac{(\phi - \phi_{\mathrm{NH}})^2}{2\delta\phi_E^2}\right]. \tag{2c}$$

Here, $O_0$ and $O_E$ are parameters that are used to vary the structure of tropical precipitation, $\phi$ denotes latitude, $\phi_{\mathrm{NH}} = 60°$ is the latitude at which perturbations of the extratropical ocean energy flux divergence (amplitude $O_E$) are centered, and $\delta\phi_0 = 16°$ and $\delta\phi_E = 7°$ are fixed widths of variations in ocean energy flux divergence. The values of $\delta\phi_E$ and $\phi_{\mathrm{NH}}$ are chosen so that the part of $\mathcal{O}$ that is antisymmetric about the equator is approximately zero within the tropics (±30° latitude), similar to what was done in Kang et al. (2008, 2009). The antisymmetric part of $\mathcal{O}$ resembles the ocean energy flux divergence of an idealized deep overturning circulation that transports heat from the Southern Hemisphere high latitudes to the Northern Hemisphere high latitudes. The value of $\delta\phi_0$ is chosen so that the spatial structure of the symmetric part of $\mathcal{O}$ approximately resembles the symmetric part of the zonal-mean ocean energy flux divergence inferred from space-based measurements and reanalysis data (e.g., Trenberth and Caron 2001; Trenberth and Fasullo 2008; Fasullo and Trenberth 2008); it also resembles the ocean energy flux divergence in a zonally symmetric wind-driven surface ocean that transports heat from the deep tropics to the subtropics (Klinger and Marotzke 2000; Levine and Schneider 2011). Both the symmetric and the antisymmetric components of $\mathcal{O}$ integrate to zero in an area-weighted sense.

### b. Simulation series

To test and illustrate the theory to be outlined in section 4, we performed simulations without a seasonal cycle, similar to the ones in Kang et al. (2008, 2009) and Bischoff and Schneider (2014), varying $O_0$ and $O_E$ independently from 0 to 100 W m$^{-2}$ in steps of 10 W m$^{-2}$. The range of $O_0$ is representative of equatorial ocean energy flux divergences on Earth derived from space-based measurements and reanalysis data, which take values that can exceed 100 W m$^{-2}$ (e.g., in the eastern Pacific; Trenberth and Fasullo 2008, their Fig. 2). On Earth in the zonal mean, the equatorial ocean energy flux divergence assumes values around 50–60 W m$^{-2}$ (Fasullo and Trenberth 2008, their Fig. 3). A cross-equatorial oceanic heat transport of about 0.4 PW as observed on Earth (Frierson et al. 2013; Marshall et al. 2014) corresponds to an extratropical forcing amplitude $O_E$ of about 10 W m$^{-2}$.

Figure 3 shows the cross-equatorial atmospheric moist static energy flux for all simulations. We find that it depends nearly linearly on $O_E$ and is only weakly dependent on $O_0$. Changing $O_E$ can therefore be thought of as changing the cross-equatorial atmospheric moist static energy flux, while changing $O_0$ leaves it relatively unchanged.

Figure 4 shows mass flux streamfunctions for nine representative simulations. The black triangles indicate the ITCZ position, identified as the global precipitation maximum. For all values of $O_0$, the ITCZ moves farther into the hemisphere that receives more energy as $O_E$ is

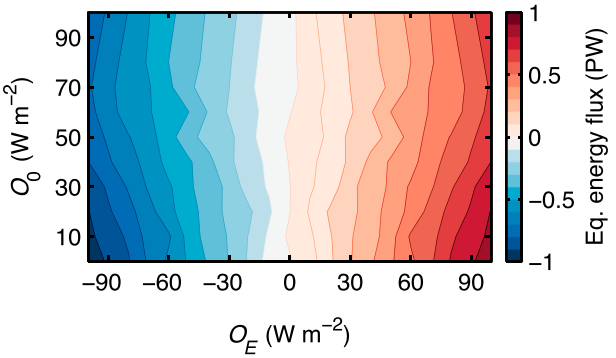


FIG. 3. Cross-equatorial atmospheric moist static energy flux for all 121 simulations. The cross-equatorial energy flux is weakly sensitive to the ocean energy flux divergence at the equator $O_0$, and it varies approximately linearly with $O_E$ for fixed $O_0$. Only simulations with positive $O_E$ were performed, and the data points are mirrored about $O_E = 0$.

increased, as was found in previous studies (e.g., Yoshimori and Broccoli 2008; Kang et al. 2008, 2009; Frierson and Hwang 2012; Donohoe et al. 2013). Concurrently, the cross-equatorial branch of the mass flux streamfunction extends farther from the ITCZ across the equator so that the subtropical terminus of the Hadley circulation in the opposite hemisphere varies little compared with the ITCZ position. The latitude of the ITCZ and of the zero of the streamfunction in the midtroposphere are approximately (within ~2°) collocated in all simulations.

## 3. ITCZ, energy flux equator, and moist static energy maximum

In the zonal and temporal mean, the ITCZ can be identified with the global precipitation maximum. Because evaporation rates $E$ around the ITCZ vary more weakly in time and space than precipitation rates $P$, the ITCZ can also be identified with the maximum of the moisture flux convergence, which in a statistically steady state balances the net precipitation $P - E$:

$$P - E = -\partial_y \langle \overline{v}\,\overline{q} \rangle . \tag{3}$$

Here, angle brackets $\langle \cdot \rangle$ denote a mass-weighted vertical integral over atmospheric columns, and overbars $\overline{(\cdot)}$ denote a zonal and temporal mean, possibly restricted to a sector of longitudes into which zonal fluxes can be neglected. We use local Cartesian coordinates for notational convenience, with $y = a\phi$, Earth's radius $a$, and latitude $\phi$; however, we perform all numerical calculations in spherical coordinates. In Earth's atmosphere, the moisture flux convergence on the right-hand side of (3) is dominated by the time- and zonal-mean circulation, but eddies also contribute (Peixoto and Oort 1992; Trenberth and Stepaniak 2003; Schneider et al. 2006). However, the eddy contributions do not substantially shift the maximum of the moisture flux convergence, so the ITCZ can be identified with the maximum of the moisture flux convergence associated with the mean meridional circulation alone, $-\partial_y \langle \overline{v}\,\overline{q} \rangle$. Further approximating the moisture flux $\langle \overline{v}\,\overline{q} \rangle$ by the mean meridional mass flux and specific humidity $q_s$ near the surface yields the following (see appendix A for details):

$$-\partial_y \langle \overline{v}\,\overline{q} \rangle \approx \frac{q_s}{2\pi a \cos(\phi)} \partial_y \Psi_{\max}(\phi), \tag{4}$$

where $\Psi_{\max}$ is the mass flux streamfunction at the level of its extremum within the Hadley cells (this level typically lies in the lower troposphere above the planetary boundary layer). The relation in (4) assumes that the near-surface specific humidity varies meridionally on larger scales than the streamfunction $\Psi$, and it neglects meridional derivatives of $\cos(\phi)$. Because the vertical mass flux is $\propto \cos^{-1}(\phi)\partial_y \Psi$, (4) implies that the maximum moisture flux convergence associated with the mean meridional circulation, and thus the ITCZ, are located where the vertical water vapor transport is maximal (cf. Donohoe et al. 2013). If, additionally, the mass flux streamfunction $\Psi$ in the vicinity of the ITCZ is approximately antisymmetric about the ITCZ, so that $\partial_{yy} \Psi_{\max} = 0$ at the ITCZ, the latitude of the ITCZ will coincide with the zero of the streamfunction: $\Psi_{\max}(\phi) = 0$. This is approximately the case in our GCM simulations (Fig. 4).

Similar reasoning based on the same approximations also provides a basis for approximately identifying the ITCZ with the energy flux equator—the zero of the atmospheric meridional energy transport (e.g., Broccoli et al. 2006; Kang et al. 2009). In the vicinity of the ITCZ, the flux of moist static energy $h = c_p T + gz + L_v q$ (symbols have their usual meanings) associated with the mean meridional circulation can be approximated as follows:

$$\langle \overline{v}\,\overline{h} \rangle \approx -\frac{\Delta h}{2\pi a \cos(\phi)} \Psi_{\max}(\phi), \tag{5}$$

where $\Delta h$ is a gross moist stability, the effective moist static energy difference between the upper and lower branches of the mean mass transport circulation (Neelin and Held 1987; Raymond et al. 2009; see appendix A for details). This relation implies that to the extent that the latitude of the ITCZ coincides with a zero of the mass flux streamfunction, where $\Psi_{\max}(\phi) = 0$ (or with locations where the gross moist stability $\Delta h$ vanishes), it also coincides with the zero of the energy flux associated with the mean meridional circulation, where $\langle \overline{v}\,\overline{h} \rangle = 0$. In other words, the atmospheric mean meridional circulation

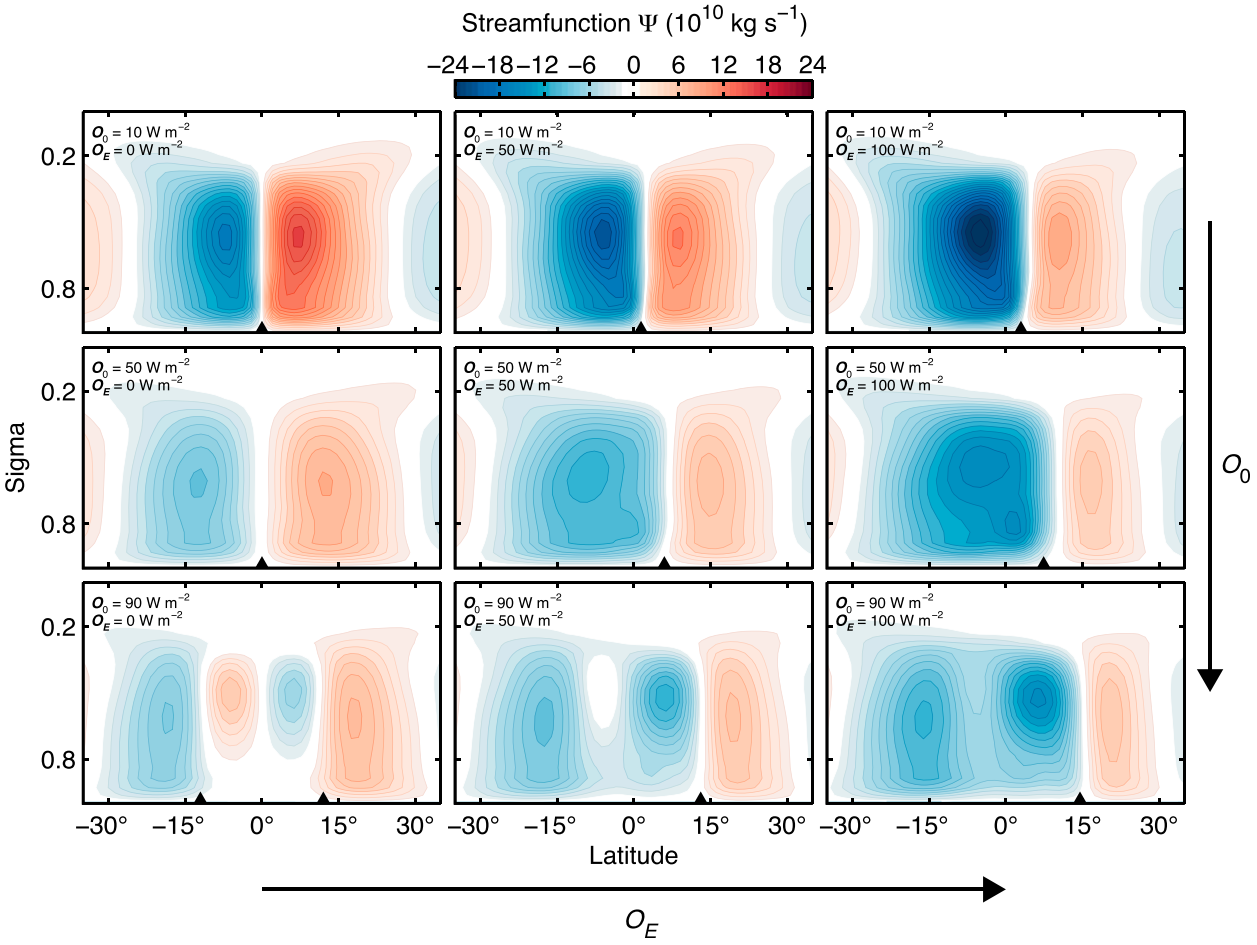


FIG. 4. Mass flux streamfunction $\Psi$ for nine simulations with different $O_0$ and $O_E$. The ocean energy flux divergence at the equator $O_0$, increases from top to bottom, and the extratropical ocean energy flux divergence $O_E$, increases from left to right. Black triangles indicate the ITCZ position for each simulation, identified as the global precipitation maximum. As $O_0$ and $O_E$ are increased, the ITCZ moves farther into the more strongly heated hemisphere. (bottom left) For the simulations with $O_E = 0$, an increase in $O_0$ eventually leads to a double ITCZ, associated with an atmospheric energy transport from the subtropics to the equator that partially compensates for the strong equatorial ocean cooling.

transports energy away from the ITCZ, and the associated energy flux changes sign at the ITCZ, like the mass flux in the upper branches of the circulation. If, additionally, eddy energy fluxes do not substantially modify the zero of the energy flux, the ITCZ approximately coincides with the energy flux equator, the zero of the total meridional energy flux $\langle \overline{vh} \rangle$ (Kang et al. 2008). This is the case in our statistically zonally symmetric GCM simulations (Fig. 5).

A further connection between the ITCZ position and energetic quantities can be made if the zero contour of the mass flux streamfunction is approximately vertical in the free troposphere, as it is in our simulations (Fig. 4) and in Earth's atmosphere (e.g., Schneider et al. 2010). In that case, the zero of the mass flux streamfunction also approximately coincides with the moist static energy maximum near the surface (Privé and Plumb 2007). This connection between the zero of the streamfunction and the near-surface moist static energy maximum arises because, in the vicinity of the ITCZ, the Hadley cells are nearly angular momentum conserving, which means that streamlines and angular momentum contours coincide (Schneider 2006; Schneider et al. 2010). A vertical zero contour of the streamfunction must coincide with an angular momentum contour, which implies that the vertical zonal wind shear (i.e., the vertical angular momentum gradient) at the latitude of the streamfunction zero must vanish. Because thermal wind balance in an atmosphere with approximately moist adiabatic stratification links the vertical zonal wind shear to gradients of near-surface moist static energy (Emanuel 1995), the net result is that a vertical zero contour of the mass flux streamfunction generally occurs at the near-surface

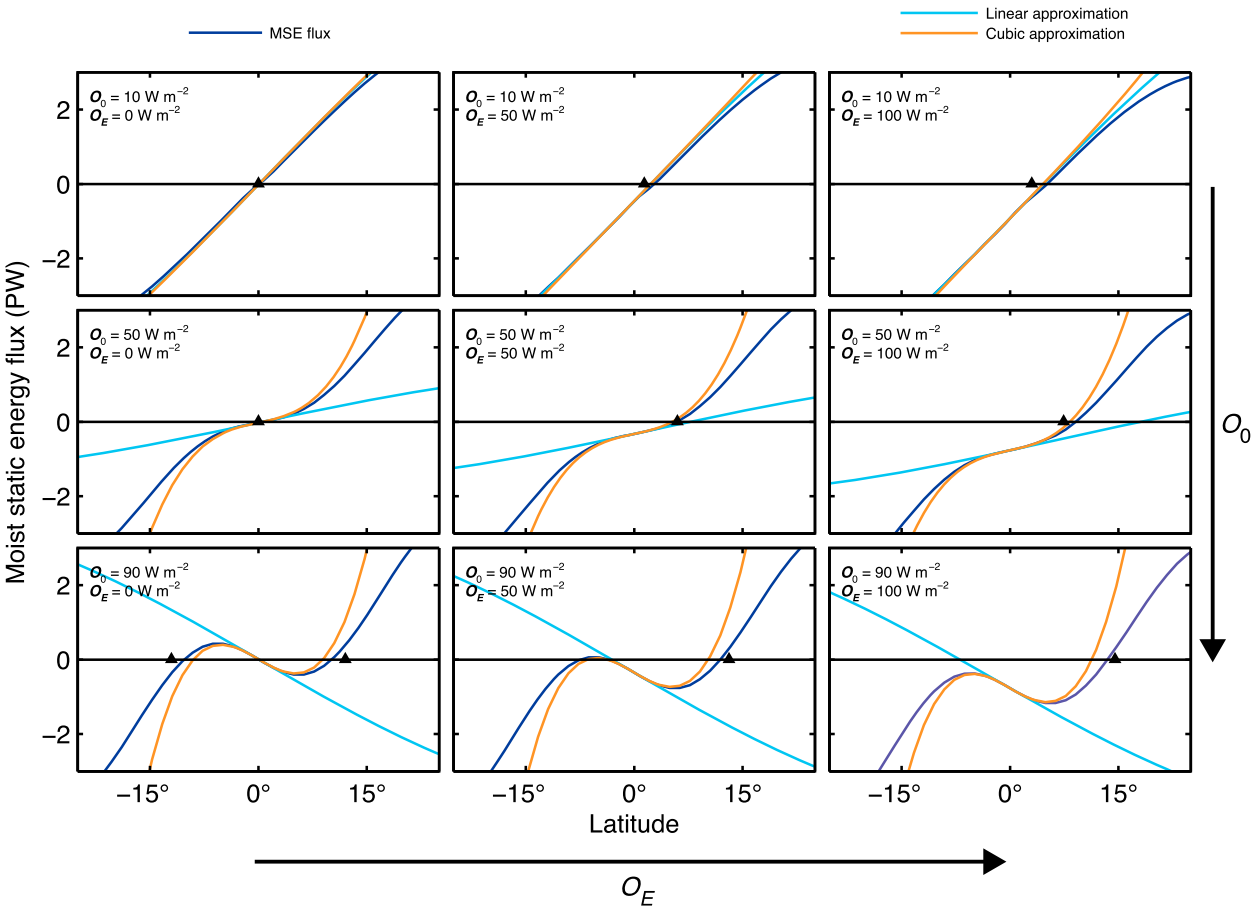


FIG. 5. Zonal-mean column moist static energy flux $\langle \overline{vh} \rangle$ (dark blue) and linear approximations (light blue) and cubic approximations (orange) for the nine simulations with different $O_0$ and $O_E$ in Fig. 4. As in Fig. 4, the black triangles indicate the ITCZ position for each simulation. The ITCZ (black triangles) and the energy flux equator (zero of blue line; $\langle \overline{vh} \rangle = 0$) vary together in all simulations. The linear approximation in (8) approximates $\langle \overline{vh} \rangle$ well for simulations with low $\mathcal{O}_0$ between $-15°$ and 15°. For $O_0 \gtrsim 50\,\mathrm{W\,m^{-2}}$, the linear approximation breaks down, and a cubic approximation [(9)] becomes necessary to capture the energy flux equator approximately.

moist static energy maximum (Privé and Plumb 2007). This is also where thermodynamic arguments suggest precipitation should be favored (Neelin and Held 1987; Sobel 2007).

Deviations from these leading-order expectations do occur. For example, the zero of the mass flux streamfunction, the energy flux equator, and the ITCZ do not always coincide when the streamfunction is strongly asymmetric about the ITCZ, such as during monsoons, when the cross-equatorial Hadley cell is much stronger than the Hadley cell that is confined to the summer hemisphere (e.g., Donohoe et al. 2013). However, meridional migrations of the ITCZ have similar magnitude as those of the energy flux equator (e.g., Kang et al. 2008; Chiang and Friedman 2012; Bischoff and Schneider 2014), and eddy contributions to derivatives of the meridional energy flux are much smaller than the contribution of the mean meridional circulation (Marshall et al. 2014). In what follows, we therefore identify the ITCZ with the energy flux equator, where $\langle \overline{vh} \rangle = 0$, and discuss the energetic constraints its position has to satisfy. A detailed study of the extent to which these constraints apply in Earth's atmosphere appears in a companion paper (Adam et al. 2016).

## 4. Energetic constraints on ITCZ position

### a. *Energy fluxes and their meridional structure*

In a statistically steady state, the zonal-mean energy balance of atmospheric columns reads as follows (e.g., Neelin and Held 1987):

$$\partial_y \langle \overline{vh} \rangle = \mathcal{S} - \mathcal{L} - \mathcal{O}, \tag{6}$$

which states that the divergence of the meridional moist static energy flux in atmospheric columns (left-hand

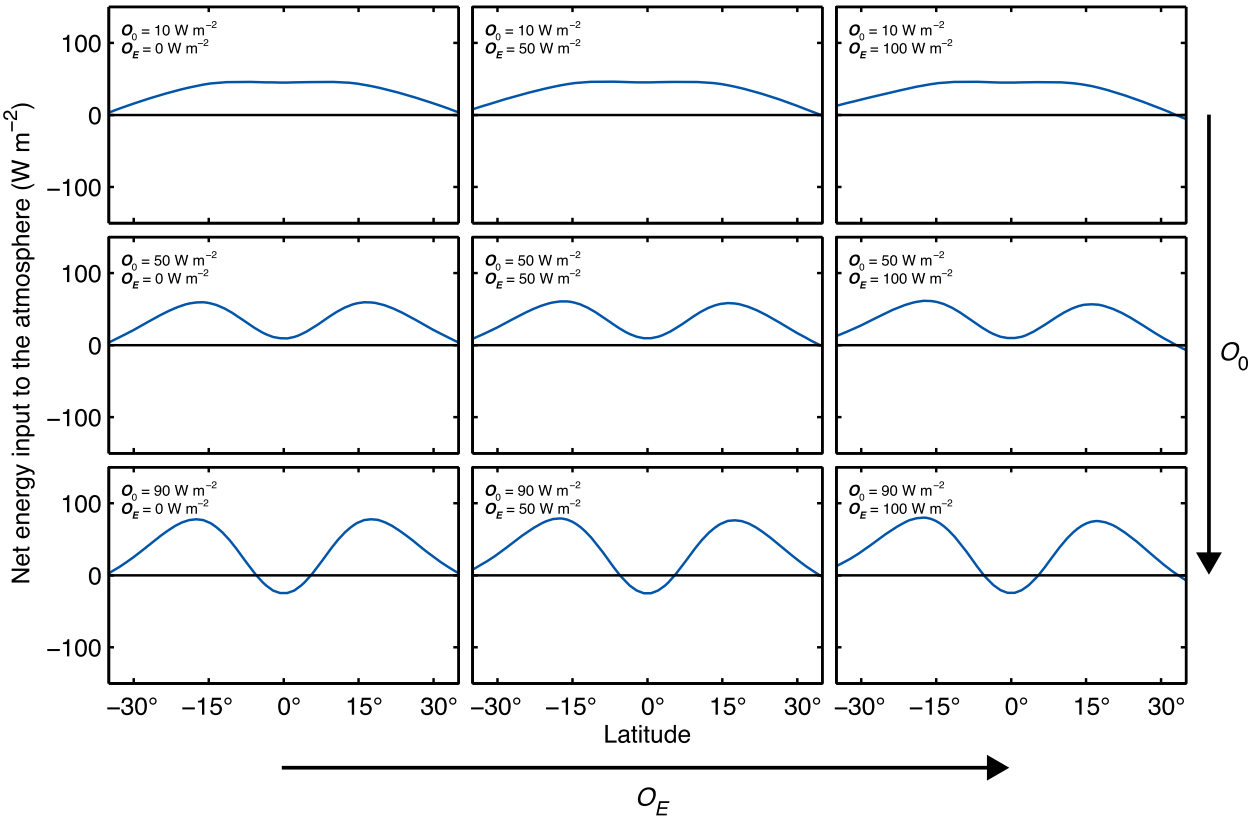


FIG. 6. Net energy input $\mathcal{S} - \mathcal{L} - \mathcal{O}$ to the tropical atmosphere for the nine simulations with different $O_0$ and $O_E$ in Figs. 4 and 5. As the ocean energy flux divergence at the equator $O_0$ is increased (going from top to bottom in columns of figure panels), the net energy input to the equatorial atmosphere decreases. At the same time, the meridional curvature of the net energy input at the equator increases. Near the equator, the net energy input remains approximately symmetric about the equator even for strongly hemispheric asymmetric forcing (large $O_E$).

side) is balanced by the net energy input to the atmosphere (right-hand side; see Fig. 6). The net energy input consists of net incoming shortwave radiation $\mathcal{S}$ and outgoing longwave radiation $\mathcal{L}$ at the top of the atmosphere as well as any energy uptake $\mathcal{O}$ at the surface. Because the ability of land surfaces to store energy is negligible, the surface energy uptake $\mathcal{O}$ occurs in the oceans. Within the oceans, this energy uptake $\mathcal{O}$ can be balanced by storage, especially on seasonal time scales, and energy flux divergence, which dominates on longer time scales. If the energy balance is not approximately in a statistically steady state, as it is in the simulations on which we focus here, energy storage in atmospheric columns must also be considered, amounting to an additional term $-\partial_t\langle e\rangle$, where $e = c_p T + L_v q$ is the moist enthalpy. This term would have to be added to $\mathcal{S} - \mathcal{L} - \mathcal{O}$ on the right-hand side; our considerations in what follows would remain valid with this modified right-hand side.

The atmospheric energy balance in (6) implies that the atmosphere transports energy from regions of positive net energy input (e.g., the tropics) to regions of negative net energy input (e.g., the extratropics). As in Bischoff and Schneider (2014), we expand the zonal-mean energy flux $\langle\overline{vh}\rangle$ around the equator''

$$\langle\overline{vh}\rangle_\phi = \langle\overline{vh}\rangle_0 + a\partial_y\langle\overline{vh}\rangle_0\phi + \frac{1}{2}a^2\partial_{yy}\langle\overline{vh}\rangle_0\phi^2 + \frac{1}{6}a^3\partial_{yyy}\langle\overline{vh}\rangle_0\phi^3 + O(\phi^4), \tag{7}$$

with expressions with subscript 0 evaluated at the equator. The equator is a convenient reference point because in our GCM simulations the quadratic term is negligible compared to the cubic term because $\mathcal{S}$, $\mathcal{L}$, and $\mathcal{O}$ are nearly symmetric about the equator, so that $\partial_{yy}\langle\overline{vh}\rangle_0 = \partial_y(\mathcal{S} - \mathcal{L} - \mathcal{O})_0$ is small (see Fig. 6). The same is true for Earth's atmosphere in the annual mean. According to the energy flux data described in Fasullo and Trenberth (2008) and Trenberth and Fasullo (2008) [data are available in NCAR Staff (2014)], the ratio of the coefficients of the quadratic and cubic terms is small:

$$3\partial_{yy}\langle\overline{vh}\rangle_0/[a\partial_{yyy}\langle\overline{vh}\rangle_0] \lesssim 0.02.$$

This implies that for an ITCZ more than ~0.04 rad ≈ 2° off the equator, the quadratic term is at least a factor of 2 smaller than the cubic term (and for an ITCZ closer to the equator, both likely are negligible compared to the linear term). The underlying physical reason is that the absorbed solar radiation $\mathcal{S}$ is almost symmetric about the equator in the annual mean, except for the modulation through shortwave scattering by the ITCZ clouds themselves (Stephens et al. 2015). The outgoing longwave radiation is almost symmetric about the equator, even seasonally, except for the modulation through longwave absorption by the ITCZ clouds and by the enhanced humidity of the atmosphere near the ITCZ. The approximate symmetry of the longwave radiation arises because temperatures in the free troposphere vary approximately symmetrically about the equator, even when the ITCZ is far off the equator and the Hadley circulation is strongly asymmetric (Lindzen and Hou 1988; Schneider et al. 2014). Modulations of $\mathcal{S}$ and $\mathcal{L}$ by the ITCZ clouds largely cancel because the shortwave and longwave effects of deep clouds nearly cancel (Harrison et al. 1990; Loeb et al. 2009; Stephens et al. 2015). Asymmetries in $\mathcal{O}$ are not large enough to offset the near symmetry of $\mathcal{S}-\mathcal{L}$. Therefore, the quadratic term in the expansion in (7) may often be negligible, and we neglect it in what follows.

Using the atmospheric energy balance in (6), we can then rewrite (7) to get, at first order, the linear approximation for the moist static energy flux near the equator used in Bischoff and Schneider (2014) and Schneider et al. (2014):

$$\langle\overline{vh}\rangle_\phi \approx \langle\overline{vh}\rangle_0 + a(\mathcal{S}-\mathcal{L}-\mathcal{O})_0\phi. \tag{8}$$

At third order, we get the cubic approximation without the quadratic term:

$$\langle\overline{vh}\rangle_\phi \approx \langle\overline{vh}\rangle_0 + a(\mathcal{S}-\mathcal{L}-\mathcal{O})_0\phi + \frac{a^3}{6}\partial_{yy}(\mathcal{S}-\mathcal{L}-\mathcal{O})_0\phi^3. \tag{9}$$

These equations relate the moist static energy flux at a latitude $\phi$ to the cross-equatorial moist static energy flux $\langle\overline{vh}\rangle_0$, the equatorial net energy input $(\mathcal{S}-\mathcal{L}-\mathcal{O})_0$, and its curvature $\partial_{yy}(\mathcal{S}-\mathcal{L}-\mathcal{O})_0$. The linear approximation is adequate when $\langle\overline{vh}\rangle_\phi$ varies approximately linearly with latitude around the equator. In what follows, however, we are interested in cases when $\langle\overline{vh}\rangle_\phi$ varies nonlinearly around the equator, and the cubic term in (9), with the curvature of the equatorial net energy input as coefficient, needs to be taken into account.

Figure 5 illustrates the forms the energy flux $\langle\overline{vh}\rangle_\phi$ near the equator takes in our GCM simulations with varying $O_0$ and $O_E$. It also shows the linear [(8)] and cubic [(9)] approximations. For simulations with equatorial ocean energy flux divergence $O_0 < 50\,\mathrm{W\,m^{-2}}$, the linear approximation in (8) captures the energy flux well between −15° and 15° latitude. For simulations with equatorial ocean energy flux divergence $O_0 \geq 50\,\mathrm{W\,m^{-2}}$, the cubic approximation in (9) is more accurate and captures the strong nonlinearity around the equator that develops when the ocean energy flux divergence near the equator is large. The cubic term in (9) plays an important role in controlling the ITCZ position, as shown in Fig. 5; it determines whether a single or double ITCZ forms.

The flux approximations [(8) and (9)] also lend themselves to physical interpretation of how the equatorial atmospheric energy balance impacts the ITCZ position. For example, consider a fixed southward (negative) cross-equatorial energy flux $\langle\overline{vh}\rangle_0$ (columns of Fig. 5). If the equatorial net energy input $(\mathcal{S}-\mathcal{L}-\mathcal{O})_0$ to the atmosphere is small, implying a small slope $\partial_y\langle\overline{vh}\rangle_0$ of the energy flux as a function of latitude near the equator, the region of negative energy flux has to extend far into the Northern Hemisphere, implying an energy flux equator and ITCZ far in the Northern Hemisphere. Conversely, if the equatorial net energy input to the atmosphere is larger, the region of negative energy flux does not have to extend so far into the Northern Hemisphere. Similar arguments apply to the curvature term $\partial_{yy}(\mathcal{S}-\mathcal{L}-\mathcal{O})_0$ in the cubic expansion in (9), which controls the meridional flatness of the equatorial net energy input to the atmosphere as a function of latitude. If the net energy input is flat [$\partial_{yy}(\mathcal{S}-\mathcal{L}-\mathcal{O})_0$ is small and positive], the region of negative energy flux has to extend farther into the Northern Hemisphere than when it is less flat. In other words, net energy input that is more strongly peaked near the equator favors an ITCZ closer to the equator, as is intuitive. See Fig. 6 for some examples of meridional structures of net energy inputs $\mathcal{S}-\mathcal{L}-\mathcal{O}$ in our simulations.

In what follows, we group the simulations into three categories depending on the relative importance of the terms in the cubic expansion [(9)].

#### 1) Strong positive equatorial net energy input

If the equatorial net energy input $(\mathcal{S}-\mathcal{L}-\mathcal{O})_0$ to the atmosphere is large and positive, its curvature near the equator can be neglected, and the linear approximation in (8) for the energy flux near the equator is adequate. In our simulations, this is the case when the ocean energy flux divergence is sufficiently weak ($O_0 \lesssim 50\,\mathrm{W\,m^{-2}}$;

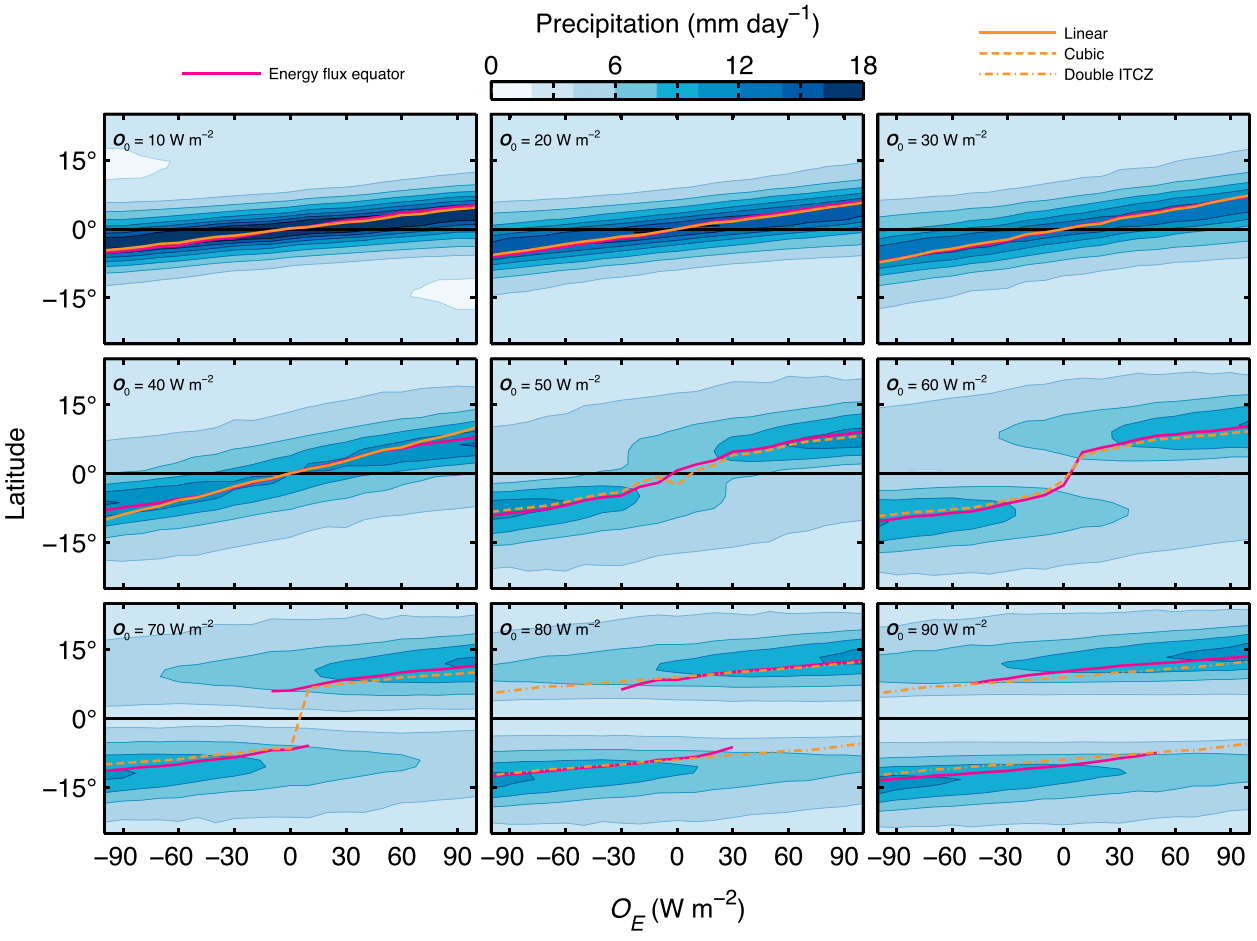


FIG. 7. Precipitation rate in all 121 simulations, for different values of the extratropical ocean energy flux divergence $O_E$ (horizontal axes) at fixed values of the ocean energy flux divergence at the equator $O_0$ (increasing from top left to bottom right). Magenta lines show the energy flux equator, where $\langle\overline{vh}\rangle = 0$. The ITCZ latitude depends approximately linearly on $O_E$ for $O_0 \lesssim 50\,\mathrm{W\,m^{-2}}$. For $O_0 \gtrsim 50\,\mathrm{W\,m^{-2}}$, the ITCZ latitude depends nonlinearly on $O_E$, as can be understood from the nonlinear dependence of $\langle\overline{vh}\rangle$ on latitude (Fig. 5). Orange lines show the approximations for the energy flux equator from (10) (linear, solid), (11) (cubic, dashed), and (13) (double ITCZ, dashed–dotted). Only simulations with positive $O_E$ were performed, and the data points are mirrored about $O_E = 0$.

Fig. 5, top row). Identifying the ITCZ with the energy flux equator where $\langle\overline{vh}\rangle = 0$, denoting its latitude by $\delta$, and solving (8) for $\delta$ gives the following:

$$\delta \approx -\frac{\langle\overline{vh}\rangle_0}{a(\mathcal{S}-\mathcal{L}-\mathcal{O})_0}. \tag{10}$$

In this case, the ITCZ latitude is anticorrelated with the cross-equatorial energy flux. The resulting approximate ITCZ latitude $\delta$ captures the variation of the actual ITCZ latitude with the amplitude $O_E$ of the extratropical ocean energy flux divergence in our simulations for $O_0 \lesssim 50\,\mathrm{W\,m^{-2}}$ (Fig. 7). The sensitivity of the ITCZ position to $O_E$ and thus to the cross-equatorial energy flux $\langle\overline{vh}\rangle_0$ (which is controlled by $O_E$) increases as $O_0$ increases and therefore $(\mathcal{S}-\mathcal{L}-\mathcal{O})_0$ decreases, in good agreement with the linear approximation in (10). This also illustrates that ITCZ shifts can arise when $(\mathcal{S}-\mathcal{L}-\mathcal{O})_0$ changes, independently of changes in the cross-equatorial energy flux $\langle\overline{vh}\rangle_0$.

### 2) WEAK POSITIVE EQUATORIAL NET ENERGY INPUT

A slightly more complicated situation arises when the cubic term in the expansion of the energy flux in (9) approximately balances the zeroth-order term, the cross-equatorial energy flux $\langle\overline{vh}\rangle_0$. In this case, the equatorial net energy input to the atmosphere is small compared to the other terms in (9), and one can solve for $\delta$ perturbatively using an asymptotic expansion (see appendix B for details). This leads to an approximation

for the energy flux equator $\delta$ that is, at leading order, given by the following:

$$\delta \approx \frac{1}{a}\left\{\frac{-6\langle\overline{vh}\rangle_0}{\partial_{yy}(\mathcal{S}-\mathcal{L}-\mathcal{O})_0}\right\}^{1/3} - \frac{2(\mathcal{S}-\mathcal{L}-\mathcal{O})_0}{\partial_{yy}(\mathcal{S}-\mathcal{L}-\mathcal{O})_0}\left\{\frac{-6\langle\overline{vh}\rangle_0}{\partial_{yy}(\mathcal{S}-\mathcal{L}-\mathcal{O})_0}\right\}^{-(1/3)}. \quad (11)$$

This approximation is only valid for nonzero $\langle\overline{vh}\rangle_0$. In the special case of $(\mathcal{S}-\mathcal{L}-\mathcal{O})_0 = 0$, it reduces to the scaling

$$\delta \propto [-\langle\overline{vh}\rangle_0]^{1/3}; \quad (12)$$

that is, a weaker dependence of ITCZ latitude on the cross-equatorial energy flux than under the linear approximation.

The approximation in (11) captures the behavior of the ITCZ in our simulations with $40\,\mathrm{W\,m^{-2}} < O_0 < 70\,\mathrm{W\,m^{-2}}$ (Fig. 7). In these simulations, the equatorial net energy input is small, $(\mathcal{S}-\mathcal{L}-\mathcal{O})_0 \lesssim 10\,\mathrm{W\,m^{-2}}$, and the linear approximation performs poorly when $O_E$ and the cross-equatorial energy flux $\langle\overline{vh}\rangle_0$ are sufficiently large (Fig. 5, middle row).

These results indicate that the ITCZ position does not necessarily vary linearly with $\langle\overline{vh}\rangle_0$ under all circumstances, as was assumed in several previous studies (e.g., Frierson and Hwang 2012; Donohoe et al. 2013). Instead, nonlinear scalings can be more appropriate. The value of the equatorial net energy input to the atmosphere (around $10\,\mathrm{W\,m^{-2}}$) where the linear approximation performs poorly in our simulations happens to be close to the corresponding value for Earth in the annual mean (Fasullo and Trenberth 2008, their Fig. 3; Marshall et al. 2014; Schneider et al. 2014).

#### 3) Negative equatorial net energy input

When the equatorial net energy input to the atmosphere $(\mathcal{S}-\mathcal{L}-\mathcal{O})_0$ is negative, the energy flux is no longer monotonically increasing with latitude, and two energy flux equators—a double ITCZ—can form on either side of the equator (Fig. 5, bottom row). Two energy flux equators can also form when the curvature $\partial_{yy}(\mathcal{S}-\mathcal{L}-\mathcal{O})_0$ becomes negative; however, ocean energy flux divergence near the equator prevents that from occurring in our simulations. When two off-equatorial energy flux equators form, the atmosphere transports energy toward the equator, away from the two off-equatorial ITCZs. When, additionally, the cubic term in the expansion in (9) approximately balances the linear term, while the cross-equatorial energy flux $\langle\overline{vh}\rangle_0$ introduces only a small correction, we can solve for the two latitudes $\delta$ of the energy flux equators using an asymptotic expansion (see appendix B), leading to the following:

$$\delta \approx \pm\frac{1}{a}\left\{-\frac{6(\mathcal{S}-\mathcal{L}-\mathcal{O})_0}{\partial_{yy}(\mathcal{S}-\mathcal{L}-\mathcal{O})_0}\right\}^{1/2} + \frac{\langle\overline{vh}\rangle_0}{3a(\mathcal{S}-\mathcal{L}-\mathcal{O})_0}. \quad (13)$$

This is valid for small cross-equatorial energy flux $\langle\overline{vh}\rangle_0$—that is, small asymmetries of the two ITCZs around the equator.

The double-ITCZ approximation in (13) captures the ITCZs in our simulations with $O_0 > 70\,\mathrm{W\,m^{-2}}$ (Fig. 7). The position of the two distinct convergence zones north and south of the equator vary linearly with $O_E$ or $\langle\overline{vh}\rangle_0$—provided the cross-equatorial energy flux is weak enough (for $\langle\overline{vh}\rangle_0 \lesssim 0.3\,\mathrm{PW}$ in our simulations). For stronger cross-equatorial energy fluxes $\langle\overline{vh}\rangle_0$, all terms in the cubic expansion in (9) are important, and $\delta$ is most conveniently calculated numerically.

Figure 8 shows the bifurcation from single to double ITCZs for different values of $O_E$. The bifurcation is most obvious for small $O_E$, where it occurs for an equatorial ocean energy flux divergence $O_0 \approx 50\,\mathrm{W\,m^{-2}}$. If $O_0$ exceeds this value, the equatorial net energy input to the atmosphere $(\mathcal{S}-\mathcal{L}-\mathcal{O})_0$ becomes negative in our simulations and a double ITCZ forms. As it happens, Earth's ocean energy uptake at the equator is close to the value at which the bifurcation occurs in our simulations; it amounts to about $O_0 \approx 54\,\mathrm{W\,m^{-2}}$ in the annual mean according to the data in Fasullo and Trenberth (2008, their Fig. 3) and Loeb et al. (2009).

### b. *Relating cross-equatorial energy flux to amplitude of extratropical forcing*

The results so far relate the ITCZ position to the atmospheric energy balance near the equator. In that sense, they are diagnostic, because the atmospheric energy balance in itself depends on the atmospheric circulation near the equator and thus on the ITCZ position. In our simulations, because the cross-equatorial energy flux depends primarily and approximately linearly on the amplitude of the imposed extratropical ocean energy flux divergence (Fig. 3), we can go a step further and express the cross-equatorial energy flux as a function of the extratropical forcing parameter $O_E$:

$$\langle\overline{vh}\rangle_0 = \gamma O_E. \quad (14)$$

Here, $\gamma \approx 1.92 \times 10^5$ m is an empirical parameter determined from a fit to the simulation with $O_0 = 50\,\mathrm{W\,m^{-2}}$ and $O_E = 100\,\mathrm{W\,m^{-2}}$. The closure in (14) can be justified by linearly relating the high-latitude temperature difference between the hemispheres to the extratropical forcing

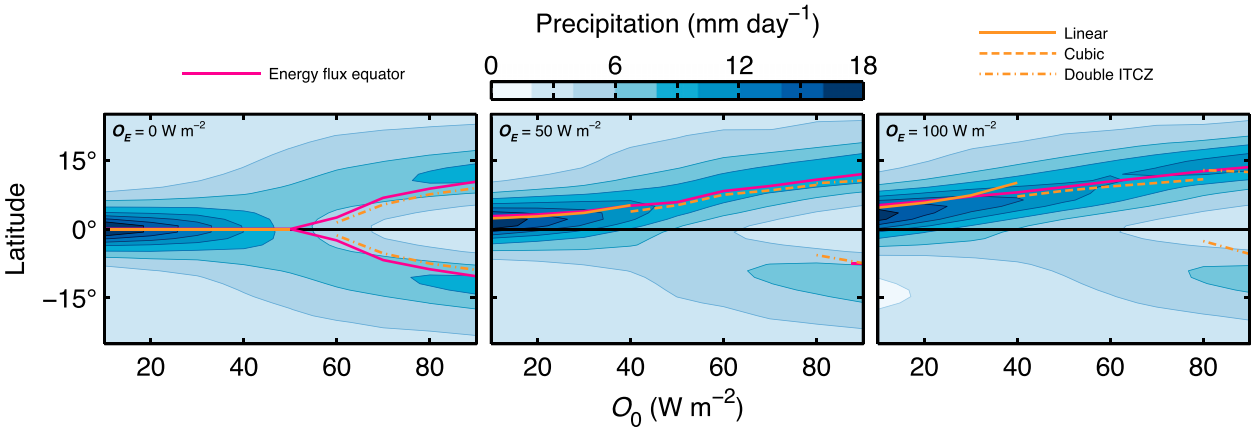


FIG. 8. Precipitation rate as in Fig. 7, but now as a function of the equatorial ocean energy flux divergence $O_0$ (horizontal axis) at fixed values of the extratropical ocean energy flux divergence $O_E$. Magenta lines show the energy flux equator, where $\langle\overline{vh}\rangle = 0$. The ITCZ latitude depends nonlinearly on $O_0$ for all values of $O_E$. For $O_0 \gtrsim 50\,\mathrm{W\,m^{-2}}$, the ITCZ bifurcates from a single- to a double-ITCZ state. Orange lines show the approximations for the energy flux equator from (10) (linear, solid), (11) (cubic, dashed), and (13) (double ITCZ, dashed–dotted). The lines shown are as in Fig. 7 and correspond to the approximations that are most appropriate for the respective simulations; (10) for simulations with $O_0 \leq 50\,\mathrm{W\,m^{-2}}$, (11) for simulations with $50 < O_0 \leq 80\,\mathrm{W\,m^{-2}}$, and (13) for simulations with $80 < O_0\,\mathrm{W\,m^{-2}}$.

amplitude $O_E$, and using a diffusive energy flux closure for extratropical eddies (e.g., Bischoff and Schneider 2014). Alternatively, one can use an energy transport efficiency parameter as in Kang et al. (2008, 2009) to justify the closure in (14). In either case, the extratropical forcing impacts the tropical circulation through the mediation by extratropical eddies that transport heat and moisture from the subtropics to the extratropics, and the parameter $\gamma$ indicates the strength of the coupling between the extratropical forcing amplitude $O_E$ and the tropical circulation.

Combining the closure in (14) with the approximations in (10), (11), or (13) for the ITCZ latitude, we arrive at expressions for $\delta$ that depend only on the forcing parameters $O_0$ and $O_E$ if changes in $\mathcal{S}$ and $\mathcal{L}$ are neglected. If we fix $\mathcal{S}$ and $\mathcal{L}$ as functions of latitude to those in the simulation with $O_0 = 50.0\,\mathrm{W\,m^{-2}}$ and $O_E = 0\,\mathrm{W\,m^{-2}}$, we obtain the approximate values $\hat{\delta}$ listed in the last column of Table 1. These approximate ITCZ positions $\hat{\delta}$ obtained solely from the external forcing parameters $O_E$ and $O_0$, using the fixed fitting parameter $\gamma$ and fixed functions $\mathcal{S}$ and $\mathcal{L}$, agree within $\lesssim 1°$ with the values of $\delta$ obtained diagnostically from the energy balance in the simulations.

This closure approach is successful in our simulations because the cross-equatorial energy flux is almost entirely determined by the amplitude of the imposed, hemispherically antisymmetric but zonally symmetric, extratropical energetic forcing. However, it will be less successful in more realistic settings when, for example, zonally asymmetric extratropical ocean energy flux divergences, which may have only a small or no projection on the zonal mean, generate stationary waves that lead to modulations of the cross-equatorial energy flux (Schneider et al. 2014). In that latter case, more sophisticated closures for the extratropical energy transport (taking stationary eddies into account) need to be used in expressions for the cross-equatorial energy flux (Bischoff and Schneider 2014).

## 5. Discussion and conclusions

### a. Summary

To study how the ITCZ depends on the energy balance near the equator, we varied the strength of the cross-equatorial atmospheric energy flux and the energy input to the equatorial atmosphere over wide ranges by perturbing an ocean energy flux divergence imposed at the lower boundary of an idealized aquaplanet GCM. As in previous studies with idealized GCMs (e.g., Kang et al. 2008, 2009), we find that the latitude of the ITCZ and of the energy flux equator coincide approximately. This remains true when two zeros of the atmospheric energy flux straddle the equator, leading to a double ITCZ.

The energy flux equator and ITCZ position are determined by how the atmospheric energy flux $\langle\overline{vh}\rangle$ varies with latitude around the equator. If the variations are approximately linear with latitude, the ITCZ displacement off the equator $\delta$ is proportional to the cross-equatorial energy flux $\langle\overline{vh}\rangle_0$ and inversely proportional to its divergence, the net energy input to the

TABLE 1. Summary of various measures of the ITCZ position for the nine simulations shown in Fig. 4. Here, $\phi_{P_{\max}}$ denotes the latitude of the precipitation maximum between −20° and 20°, $\phi_{\Psi_{\max}=0}$ denotes the latitude of the zero of the mass flux streamfunction at the level of its maximum between −20° and 20°, $\phi_{\langle\overline{vh}\rangle=0}$ denotes the latitude of the energy flux equator between −20° and 20°, $\delta$ has its usual meaning from the text, and $\hat{\delta}$ is the approximation obtained with the closure in (14) with the $\mathcal{S}$ and $\mathcal{L}$ fixed to those in the simulation with $O_0 = 50.0\,\mathrm{W\,m^{-2}}$ and $O_E = 0\,\mathrm{W\,m^{-2}}$. Where applicable, the values in parentheses show the second solution according to the double-ITCZ approximation in (13).

| $O_E$ (W m$^{-2}$) | $O_0$ (W m$^{-2}$) | $\phi_{P_{\max}}$(°) | $\phi_{\Psi_{\max}=0}$(°) | $\phi_{\langle\overline{vh}\rangle=0}$(°) | $\delta$(°) | $\hat{\delta}$(°) |
|---|---|---|---|---|---|---|
| 0 | 10 | 0.0 | 0.0 | 0.1 | 0.1 | 0.0 |
| 0 | 50 | 0.0 | 0.0 | 0.7 | — | — |
| 0 | 90 | ±12.0 | ±11.0 | ±10.2 | ±8.9 | ±9.9 |
| 50 | 10 | 1.4 | 2.4 | 2.8 | 2.3 | 1.8 |
| 50 | 50 | 6.0 | 7.0 | 5.8 | 5.2 | 5.8 |
| 50 | 90 | 13.1 | 13.5 | 11.9 | 10.0 (−8.0) | 10.8 (−8.9) |
| 100 | 10 | 3.0 | 4.9 | 5.2 | 4.6 | 3.5 |
| 100 | 50 | 7.4 | 10.5 | 9.1 | 8.3 | 8.3 |
| 100 | 90 | 14.5 | 15.5 | 13.5 | 11.2 (−6.6) | 11.7 (−8.0) |

equatorial atmosphere $(\mathcal{S} - \mathcal{L} - \mathcal{O})_0$. If higher-order terms need to be considered in a Taylor expansion of the energy flux around the equator, and if the second-order term can be neglected (as is the case in the idealized GCM and in the annual mean on Earth), more complicated situations can arise. If $(\mathcal{S} - \mathcal{L} - \mathcal{O})_0$ is small but positive, the dependence of the ITCZ position $\delta$ on $\langle\overline{vh}\rangle_0$ weakens to the third root. If $(\mathcal{S} - \mathcal{L} - \mathcal{O})_0$ becomes negative or if its curvature $\partial_{yy}(\mathcal{S} - \mathcal{L} - \mathcal{O})_0$ becomes negative, a bifurcation to double-ITCZ states occurs. The ITCZ positions $\delta$ then depend not only on $\langle\overline{vh}\rangle_0$ and $(\mathcal{S} - \mathcal{L} - \mathcal{O})_0$ but also on the curvature $\partial_{yy}(\mathcal{S} - \mathcal{L} - \mathcal{O})_0$ near the equator.

We have demonstrated the quantitative adequacy of these relations in the idealized GCM simulations, which have a statistically stationary and zonally symmetric climate. Previous studies using observations and more comprehensive climate models have documented relations between the ITCZ position and the atmospheric energy flux (e.g., Broccoli et al. 2006; Yoshimori and Broccoli 2008; Frierson and Hwang 2012; Donohoe et al. 2013; Hwang et al. 2013). This suggests that our results may apply to Earth's atmosphere, at least in the zonal and long-term mean. A detailed study of their applicability to seasonal and interannual variations of the ITCZ appears in a companion paper (Adam et al. 2016). Several broader implications for the interpretation of climate records and climate modeling can already be seen.

### b. *Implications for interpreting climate records*

Our results provide a framework within which a broad range of ITCZ variations can be interpreted and previous results can be recontextualized. For example, paleoclimatological evidence and observations suggest that the ITCZ has migrated meridionally in the past and that it may do so again in the future in response to anthropogenic climate changes (e.g., Folland et al. 1986; Dai and Wigley 2000; Rotstayn and Lohmann 2002; Giannini et al. 2003; Chiang and Bitz 2005; Held et al. 2005; Sachs et al. 2009; Hwang et al. 2013; McGee et al. 2014; Schneider et al. 2014). Often such ITCZ migrations are interpreted in terms of changes in cross-equatorial atmospheric energy fluxes, triggered, for example, by changes in the albedo of one hemisphere that may be caused by changes in glaciation or aerosol loadings. Our results show that the ITCZ position does not depend only on the cross-equatorial energy flux and factors that may influence it, such as the interhemispheric temperature contrast (e.g., Chiang and Bitz 2005; Chiang and Friedman 2012). The ITCZ position is also controlled by the equatorial net energy input and, especially if that is small or negative, by its higher derivatives with respect to latitude. The latter can modulate the sensitivity of the ITCZ to changes in the cross-equatorial atmospheric energy flux. This may account, for example, for the double ITCZ that arises during spring in the eastern Pacific (Fig. 1), which collapses to a single ITCZ south of the equator during El Niño (Zhang 2001; Xie and Yang 2014). Consistent with our analysis, the equatorial net energy input to the atmosphere in the eastern Pacific is usually negative (Trenberth and Fasullo 2008) but becomes positive during strong El Niños (Adam et al. 2016), when even the South Pacific convergence zone—an extreme double ITCZ—can collapse onto the equator (Cai et al. 2012; Borlace et al. 2014).

Stated generally, a linear relation between the ITCZ position and the cross-equatorial atmospheric energy flux cannot usually be expected. Dependencies of the ITCZ position on the equatorial net energy input to the atmosphere and its derivatives should be examined.

### c. Implications for climate modeling

The ITCZ position depends on the equatorial net energy input to the atmosphere $(\mathcal{S} - \mathcal{L} - \mathcal{O})_0$, which is a small residual of large terms (Schneider et al. 2014). For Earth in the annual and zonal mean, the net incoming shortwave radiation is about $\mathcal{S}_0 = 323\,\mathrm{W\,m^{-2}}$, the outgoing longwave radiation is about $\mathcal{L}_0 = 251\,\mathrm{W\,m^{-2}}$, and the ocean energy uptake is about $\mathcal{O}_0 = 54\,\mathrm{W\,m^{-2}}$, leaving the relatively small residual $(\mathcal{S} - \mathcal{L} - \mathcal{O})_0 \approx 18\,\mathrm{W\,m^{-2}}$. This alone makes the ITCZ position sensitive to small biases in climate models' energy balance, such as may occur through biases in cloud shortwave and longwave effects. Beyond that, our results show that the ITCZ position can also depend, for example, on the curvature of $(\mathcal{S} - \mathcal{L} - \mathcal{O})$ as a function of latitude. This makes the ITCZ position sensitive, for example, to biases in the sharpness of equatorial ocean upwelling and likely leads to a dependence of the ITCZ position on model resolution.

For example, Earth's ITCZ appears to be close to the boundary at which $(\mathcal{S} - \mathcal{L} - \mathcal{O})$ becomes negative and the bifurcation to a double-ITCZ state occurs. Relatively small biases in the energy balance may thus lead to the well-known double-ITCZ bias of climate models (Lin 2007). Extratropical model biases likely contribute to this tropical bias (e.g., Hwang and Frierson 2013). But tropical biases—for example, in cloud radiative effects (e.g., Zhang and Wang 2006; Kang et al. 2009; Voigt and Shaw 2015) or ocean energy uptake—may also play a role, with cloud feedbacks being especially important. Consistent with our framework, the double-ITCZ bias in climate models appears to be related to a cool bias of equatorial sea surface temperatures (Ashfaq et al. 2011; Vannière et al. 2014), suggesting a low bias of the equatorial net energy input to the atmosphere. Because the equatorial net energy input to the atmosphere depends on the ocean energy uptake, climate models with a fixed ocean energy transport or with fixed sea surface temperatures can give a different structure of the ITCZ and how it changes with climate compared with models with interactive ocean energy transport (Vannière et al. 2014).

An analysis of climate model biases within the framework we presented here promises to be a fruitful avenue of research. This may help identify the causes of the biases.

### d. Open questions

Relating the energy flux equator and ITCZ position in greater detail and generality than has been done previously to the energy balance of the atmosphere represents progress. Nonetheless, the energy balance is merely one identity the atmosphere has to satisfy; a Taylor expansion of it around the equator provides diagnostic relations for the ITCZ position but does not represent a closed dynamical theory (Schneider et al. 2014). The quantities entering the energy balance themselves depend on the atmospheric circulation and thus on the ITCZ position. For example, the net energy input depends on the atmospheric circulations responsible for the energy transport and its divergence, which in turn depend on where the ITCZ is located (e.g., Lindzen and Hou 1988; Chou and Neelin 2001, 2003; Sobel and Neelin 2006; Neelin 2007; Sobel 2007; Schneider and Bordoni 2008; Bordoni and Schneider 2008). A closed theory of the ITCZ must, for example, also take the angular momentum balance into account, both near the surface (e.g., Lindzen and Nigam 1987; Waliser and Somerville 1994; Schneider and Bordoni 2008) and in the free troposphere (e.g., Schneider et al. 2010). The angular momentum balance in part controls the mean meridional mass flux $\Psi_{\max}$ (e.g., Schneider 2006), which together with the gross moist stability enters the energy balance through the relation in (5) between mass fluxes and energy fluxes. The angular momentum balance controlling the mean meridional mass flux in turn depends on eddy fluxes of angular momentum (Walker and Schneider 2006), which thus also can affect the ITCZ position through the energy transport associated with the mean meridional circulation. However, such dependencies are only implicit if one focuses on the energy balance alone. How the constraints from the energy balance and angular momentum balance are to be coupled in a closed theory is a largely unresolved question.

In addition to such unresolved questions, the ITCZ on Earth is not zonally symmetric, so a local theory for an ITCZ position that depends on longitude is needed. This may be accomplished by including zonal moist static energy fluxes in versions of the energy balance in (6) averaged over finite longitudinal sectors.

Also appearing in the relation in (5) between mass fluxes and energy fluxes is the gross moist stability (Neelin and Held 1987; Raymond et al. 2009). For the gross moist stability, likewise, no closed and generally adequate theory exists yet (Hill et al. 2015). Additionally, the ITCZ is not always collocated with the energy flux equator. Resolving these outstanding questions remains as a challenge to dynamicists.

*Acknowledgments.* This research was supported by a grant from the National Science Foundation (AGS-1049201). The idealized GCM simulations were performed on Caltech's Geological and Planetary Sciences CITerra and on ETH Zurich's EULER computing clusters. We thank Simona Bordoni and

Anne Laraia for helpful discussions of drafts of this paper. We also acknowledge the World Climate Research Programme's Working Group on Coupled Modelling, which is responsible for CMIP, and we thank the climate modeling groups for producing and making available their model output, which we used in Fig. 1. For CMIP, the U.S. Department of Energy's Program for Climate Model Diagnosis and Intercomparison provides coordinating support and led development of software infrastructure in partnership with the Global Organization for Earth System Science Portals. We also thank John Fasullo and Kevin Trenberth from the National Center for Atmospheric Research for providing the energy flux data (retrieved from https://climatedataguide.ucar.edu/climate-data/era-interim-derived-components) we used in some of the estimates in the text.

## APPENDIX A

### Relating Energy, Moisture, and Mass Transports

The column-integrated moisture flux associated with the mean meridional circulation in a statistically steady state can be approximated as follows:

$$\langle \overline{v}\,\overline{q}\rangle = \int_0^{p_s} \mathcal{H}(\overline{v})\overline{v}\,\overline{q}\frac{dp}{g} + \int_0^{p_s} \mathcal{H}(-\overline{v})\overline{v}\,\overline{q}\frac{dp}{g} \quad \text{(A1a)}$$

$$\approx q_t \int_0^{p(\overline{v}=0)} \overline{v}\frac{dp}{g} + q_s \int_{p(\overline{v}=0)}^{p_s} \overline{v}\frac{dp}{g} \quad \text{(A1b)}$$

$$= (q_t - q_s)\int_0^{p(\overline{v}=0)} \overline{v}\frac{dp}{g} \quad \text{(A1c)}$$

$$\approx -\frac{q_s \Psi_{\max}(\phi)}{2\pi a \cos(\phi)}. \quad \text{(A1d)}$$

Here, we have used the mean value theorem for integrals to go from the first to the second line, $q_s$ and $q_t$ are representative specific humidities in the lower branch and upper branch of the overturning circulation (divided at the level at which the mean meridional flow vanishes), and $\mathcal{H}$ denotes the Heaviside function. Mass conservation in atmospheric columns was used in going from the second to the third line. And because the specific humidity in the upper branch is much lower than that in the lower branch ($q_t \ll q_s$), the final approximate equality follows, with the mass flux streamfunction $\Psi(p, \phi) = 2\pi a \cos(\phi)\int_0^p \overline{v}dp/g$.

Similarly, the column-integrated energy flux associated with the mean meridional circulation can be approximated as follows:

$$\langle \overline{v}\,\overline{h}\rangle = \int_0^{p_s} \mathcal{H}(\overline{v})\overline{v}\,\overline{h}\frac{dp}{g} + \int_0^{p_s} \mathcal{H}(-\overline{v})\overline{v}\,\overline{h}\frac{dp}{g} \quad \text{(A2a)}$$

$$\approx \frac{(h_t - h_s)\Psi_{\max}(\phi)}{2\pi a \cos(\phi)} \quad \text{(A2b)}$$

$$\approx \frac{\Delta h \Psi_{\max}(\phi)}{2\pi a \cos(\phi)}, \quad \text{(A2c)}$$

where $\Delta h = h_t - h_s$ is a gross moist stability (Neelin and Held 1987; Raymond et al. 2009).

## APPENDIX B

### Asymptotic Approximation for the ITCZ Position

Section 4 presented asymptotic approximations to the ITCZ position, which were approximate roots $\delta$ of a third-order polynomial of the following form:

$$0 = A + B\delta + C\delta^3, \quad \text{(B1)}$$

where $A = \langle \overline{vh}\rangle_0$, $B = a\partial_y\langle \overline{vh}\rangle_0$, and $C = (1/6)a^3\partial_{yyy}\langle \overline{vh}\rangle_0$. If $C = 0$, then (B1) can be solved straightforwardly by

$$\delta = -\frac{A}{B}, \quad \text{(B2)}$$

corresponding to the approximation in (10) for strong positive equatorial net energy input.

For weak positive equatorial net energy input (small $B$), when the cubic term in the expansion of the energy flux in (9) approximately balances the constant term, we can expand $\delta$ in a power series in $B$:

$$\delta = \delta_0 + \delta_1 B + \cdots. \quad \text{(B3)}$$

Inserting this series for $\delta$ into (B1) gives at zeroth order

$$0 = A + C\delta_0^3 \quad \Rightarrow \quad \delta_0 = \left(-\frac{A}{C}\right)^{1/3}, \quad \text{(B4)}$$

and at first order

$$0 = B\delta_0 + 3C\delta_0^2 B\delta_1 \quad \Rightarrow \quad \delta_1 = -\frac{1}{3C\delta_0}. \quad \text{(B5)}$$

If $A \neq 0$, $C \neq 0$, the perturbation expansion for $\delta$ is then given by

$$\delta \approx \delta_0\left(1 + \frac{\delta_1}{\delta_0}B\right) = \left(-\frac{A}{C}\right)^{1/3}\left[1 - \frac{1}{3}\frac{B}{C}\left(-\frac{C}{A}\right)^{2/3}\right], \quad \text{(B6)}$$

which corresponds to the approximation in (11).

For negative equatorial net energy input and when $A$ is small, the cubic term in the expansion of the energy flux in (9) approximately balances the linear term, and we can expand $\delta$ in a power series in $A$:

$$\delta = \delta_0 + \delta_1 A + \cdots . \tag{B7}$$

Inserting this series for $\delta$ into (B1) gives at zeroth order

$$0 = (B + C\delta_0^2)\delta_0 \quad \Rightarrow \quad \delta_0 = 0 \quad \text{or} \quad \delta_0 = \pm\left(-\frac{B}{C}\right)^{1/2}, \tag{B8}$$

and at first order ($\delta_0 \neq 0$)

$$0 = A + 3C\delta_0^2 A\delta_1 \quad \Rightarrow \quad \delta_1 = -\frac{1}{3C\delta_0^2} = \frac{1}{3B}. \tag{B9}$$

If $B \neq 0$, $C \neq 0$, the perturbation expansion for $\delta$ is then given by

$$\delta \approx \pm\left(-\frac{B}{C}\right)^{1/2} + \frac{A}{3B}, \tag{B10}$$

which corresponds to the approximation in (13).

## REFERENCES


Adam, O., T. Bischoff, and T. Schneider, 2016: Seasonal and interannual variations of the energy flux equator and ITCZ in present climate. Part I: Zonally averaged ITCZ position. *J. Climate*, doi:10.1175/JCLI-D-15-0512.1, in press.

Ashfaq, M., C. B. Skinner, and N. S. Diffenbaugh, 2011: Influence of SST biases on future climate change projections. *Climate Dyn.*, **36**, 1303–1319, doi:10.1007/s00382-010-0875-2.

Bischoff, T., and T. Schneider, 2014: Energetic constraints on the position of the intertropical convergence zone. *J. Climate*, **27**, 4937–4951, doi:10.1175/JCLI-D-13-00650.1.

Bordoni, S., and T. Schneider, 2008: Monsoons as eddy-mediated regime transitions of the tropical overturning circulation. *Nat. Geosci.*, **1**, 515–519, doi:10.1038/ngeo248.

Borlace, S., A. Santoso, W. Cai, and M. Collins, 2014: Extreme swings of the South Pacific convergence zone and the different types of El Niño events. *J. Geophys. Res.*, **41**, 4695–4703, doi:10.1002/2014GL060551.

Broccoli, A. J., K. A. Dahl, and R. J. Stouffer, 2006: Response of the ITCZ to Northern Hemisphere cooling. *Geophys. Res. Lett.*, **33**, L01702, doi:10.1029/2005GL024546.

Cai, W., and Coauthors, 2012: More extreme swings of the South Pacific convergence zone due to greenhouse warming. *Nature*, **488**, 365–369, doi:10.1038/nature11358.

Chiang, J. C. H., and C. M. Bitz, 2005: Influence of high latitude ice cover on the marine intertropical convergence zone. *Climate Dyn.*, **25**, 477–496, doi:10.1007/s00382-005-0040-5.

——, and A. R. Friedman, 2012: Extratropical cooling, interhemispheric thermal gradients, and tropical climate change. *Annu. Rev. Earth Planet. Sci.*, **40**, 383–412, doi:10.1146/annurev-earth-042711-105545.

Chou, C., and J. D. Neelin, 2001: Mechanisms limiting the southward extent of the South American summer monsoon. *Geophys. Res. Lett.*, **28**, 2433–2436, doi:10.1029/2000GL012138.

——, and ——, 2003: Mechanisms limiting the northward extent of the northern summer monsoons over North America, Asia, and Africa. *J. Climate*, **16**, 406–425, doi:10.1175/1520-0442(2003)016<0406:MLTNEO>2.0.CO;2.

Cvijanovic, I., and J. C. H. Chiang, 2013: Global energy budget changes to high latitude North Atlantic cooling and the tropical ITCZ response. *Climate Dyn.*, **40**, 1435–1452, doi:10.1007/s00382-012-1482-1.

Dai, A., and T. M. L. Wigley, 2000: Global patterns of ENSO-induced precipitation. *Geophys. Res. Lett.*, **27**, 1283–1286, doi:10.1029/1999GL011140.

Donohoe, A., J. Marshall, D. Ferreira, and D. McGee, 2013: The relationship between ITCZ location and cross equatorial atmospheric heat transport: From the seasonal cycle to the Last Glacial Maximum. *J. Climate*, **26**, 3597–3618, doi:10.1175/JCLI-D-12-00467.1.

Emanuel, K. A., 1995: On thermally direct circulations in moist atmospheres. *J. Atmos. Sci.*, **52**, 1529–1534, doi:10.1175/1520-0469(1995)052<1529:OTDCIM>2.0.CO;2.

Fasullo, J. T., and K. E. Trenberth, 2008: The annual cycle of the energy budget. Part II: Meridional structures and poleward transports. *J. Climate*, **21**, 2313–2325, doi:10.1175/2007JCLI1936.1.

Folland, C. K., T. N. Palmer, and D. E. Parker, 1986: Sahel rainfall and worldwide sea temperatures, 1901–85. *Nature*, **320**, 602–607, doi:10.1038/320602a0.

Friedman, A. R., Y.-T. Hwang, J. C. Chiang, and D. M. W. Frierson, 2013: Interhemispheric temperature asymmetry over the twentieth century and in future projections. *J. Climate*, **26**, 5419–5433, doi:10.1175/JCLI-D-12-00525.1.

Frierson, D. M. W., 2007: The dynamics of idealized convection schemes and their effect on the zonally averaged tropical circulation. *J. Atmos. Sci.*, **64**, 1959–1976, doi:10.1175/JAS3935.1.

——, and Y.-T. Hwang, 2012: Extratropical influence on ITCZ shifts in slab ocean simulations of global warming. *J. Climate*, **25**, 720–733, doi:10.1175/JCLI-D-11-00116.1.

——, and Coauthors, 2013: Contribution of ocean overturning circulation to tropical rainfall peak in the Northern Hemisphere. *Nat. Geosci.*, **6**, 940–944, doi:10.1038/ngeo1987.

Giannini, A., R. Saravanan, and P. Chang, 2003: Oceanic forcing of Sahel rainfall on interannual to interdecadal time scales. *Science*, **302**, 1027–1030, doi:10.1126/science.1089357.

Harrison, E. F., P. Minnis, B. R. Barkstrom, V. Ramanathan, R. D. Cess, and G. G. Gibson, 1990: Seasonal variation of cloud radiative forcing derived from the Earth Radiation Budget Experiment. *J. Geophys. Res.*, **95**, 18 687–18 703, doi:10.1029/JD095iD11p18687.

Held, I. M., T. L. Delworth, J. Lu, K. L. Findell, and T. R. Knutson, 2005: Simulation of Sahel drought in the 20th and 21st centuries. *Proc. Natl. Acad. Sci. USA*, **102**, 17 891–17 896, doi:10.1073/pnas.0509057102.

Hill, S. A., Y. Ming, and I. M. Held, 2015: Mechanisms of forced tropical meridional energy flux change. *J. Climate*, **28**, 1725–1742, doi:10.1175/JCLI-D-14-00165.1.

Hwang, Y.-T., and D. M. W. Frierson, 2013: Link between the double-intertropical convergence zone problem and cloud biases over the Southern Ocean. *Proc. Natl. Acad. Sci. USA*, **110**, 4935–4940, doi:10.1073/pnas.1213302110.

——, ——, and S. M. Kang, 2013: Anthropogenic sulfate aerosol and the southward shift of tropical precipitation in the late 20th century. *Geophys. Res. Lett.*, **40**, 2845–2850, doi:10.1002/grl.50502.

Kang, S. M., I. M. Held, D. M. W. Frierson, and M. Zhao, 2008: The response of the ITCZ to extratropical thermal forcing: Idealized slab-ocean experiments with a GCM. *J. Climate*, **21**, 3521–3532, doi:10.1175/2007JCLI2146.1.

——, D. M. W. Frierson, and I. M. Held, 2009: The tropical response to extratropical thermal forcing in an idealized GCM: The importance of radiative feedbacks and convective parameterization. *J. Atmos. Sci.*, **66**, 2812–2827, doi:10.1175/2009JAS2924.1.

Klinger, B. A., and J. Marotzke, 2000: Meridional heat transport by the subtropical cell. *J. Phys. Oceanogr.*, **30**, 696–705, doi:10.1175/1520-0485(2000)030<0696:MHTBTS>2.0.CO;2.

Levine, X. J., and T. Schneider, 2011: Response of the Hadley circulation to climate change in an aquaplanet GCM coupled to a simple representation of ocean heat transport. *J. Atmos. Sci.*, **68**, 769–783, doi:10.1175/2010JAS3553.1.

Lin, J.-L., 2007: The double-ITCZ problem in IPCC AR4 coupled GCMs: Ocean–atmosphere feedback analysis. *J. Climate*, **20**, 4497–4525, doi:10.1175/JCLI4272.1.

Lindzen, R. S., and S. Nigam, 1987: On the role of sea surface temperature gradients in forcing low-level winds and convergence in the tropics. *J. Atmos. Sci.*, **44**, 2418–2436, doi:10.1175/1520-0469(1987)044<2418:OTROSS>2.0.CO;2.

——, and A. Y. Hou, 1988: Hadley circulations for zonally averaged heating centered off the equator. *J. Atmos. Sci.*, **45**, 2416–2427, doi:10.1175/1520-0469(1988)045<2416:HCFZAH>2.0.CO;2.

Liu, Z., D. Ostrenga, W. Teng, and S. Kempler, 2012: Tropical Rainfall Measuring Mission (TRMM) precipitation data and services for research and applications. *Bull. Amer. Meteor. Soc.*, **93**, 1317–1325, doi:10.1175/BAMS-D-11-00152.1.

Loeb, N. G., B. A. Wielicki, D. R. Doelling, G. L. Smith, D. F. Keyes, S. Kato, N. Manalo-Smith, and T. Wong, 2009: Toward optimal closure of the Earth's top-of-atmosphere radiation budget. *J. Climate*, **22**, 748–766, doi:10.1175/2008JCLI2637.1.

Marshall, J., A. Donohoe, D. Ferreira, and D. McGee, 2014: The ocean's role in setting the mean position of the inter-tropical convergence zone. *Climate Dyn.*, **42**, 1967–1979, doi:10.1007/s00382-013-1767-z.

McGee, D., A. Donohoe, J. Marshall, and D. Ferreira, 2014: Changes in ITCZ location and cross-equatorial heat transport at the Last Glacial Maximum, Heinrich Stadial 1, and the mid-Holocene. *Earth Planet. Sci. Lett.*, **390**, 69–79, doi:10.1016/j.epsl.2013.12.043.

Merlis, T. M., T. Schneider, S. Bordoni, and I. Eisenman, 2013: Hadley circulation response to orbital precession. Part I: Aquaplanets. *J. Climate*, **26**, 740–753, doi:10.1175/JCLI-D-11-00716.1.

NCAR Staff, Eds., 2014: The climate data guide: ERA-Interim: Derived components. NCAR/UCAR, accessed 2 January 2014. [Available online at https://climatedataguide.ucar.edu/climate-data/era-interim-derived-components.]

Neelin, J. D., 2007: Moist dynamics of tropical convection zones in monsoons, teleconnections, and global warming. *The Global Circulation of the Atmosphere*, T. Schneider and A. H. Sobel, Eds., Princeton University Press, 267–301.

——, and I. M. Held, 1987: Modeling tropical convergence based on the moist static energy budget. *Mon. Wea. Rev.*, **115**, 3–12, doi:10.1175/1520-0493(1987)115<0003:MTCBOT>2.0.CO;2.

O'Gorman, P. A., and T. Schneider, 2008: The hydrological cycle over a wide range of climates simulated with an idealized GCM. *J. Climate*, **21**, 3815–3832, doi:10.1175/2007JCLI2065.1.

Peixoto, J. P., and A. H. Oort, 1992: *Physics of Climate.* 1st ed. American Institute of Physics, 520 pp.

Privé, N. C., and R. A. Plumb, 2007: Monsoon dynamics with interactive forcing. Part I: Axisymmetric studies. *J. Atmos. Sci.*, **64**, 1417–1430, doi:10.1175/JAS3916.1.

Raymond, D. J., S. Sessions, A. H. Sobel, and Z. Fuchs, 2009: The mechanics of gross moist stability. *J. Adv. Model. Earth Syst.*, **1**, 9, doi:10.3894/JAMES.2009.1.9.

Rotstayn, L. D., and U. Lohmann, 2002: Tropical rainfall trends and the indirect aerosol effect. *J. Climate*, **15**, 2103–2116, doi:10.1175/1520-0442(2002)015<2103:TRTATI>2.0.CO;2.

Sachs, J. P., D. Sachse, R. H. Smittenberg, Z. Zhang, D. S. Battisti, and S. Golubic, 2009: Southward movement of the Pacific intertropical convergence zone AD 1400–1850. *Nat. Geosci.*, **2**, 519–525, doi:10.1038/ngeo554.

Schneider, T., 2006: The general circulation of the atmosphere. *Annu. Rev. Earth Planet. Sci.*, **34**, 655–688, doi:10.1146/annurev.earth.34.031405.125144.

——, and S. Bordoni, 2008: Eddy-mediated regime transitions in the seasonal cycle of a Hadley circulation and implications for monsoon dynamics. *J. Atmos. Sci.*, **65**, 915–934, doi:10.1175/2007JAS2415.1.

——, K. L. Smith, P. A. O'Gorman, and C. C. Walker, 2006: A climatology of tropospheric zonal-mean water vapor fields and fluxes in isentropic coordinates. *J. Climate*, **19**, 5918–5933, doi:10.1175/JCLI3931.1.

——, P. A. O'Gorman, and X. J. Levine, 2010: Water vapor and the dynamics of climate changes. *Rev. Geophys.*, **48**, RG3001, doi:10.1029/2009RG000302.

——, T. Bischoff, and G. H. Haug, 2014: Migrations and dynamics of the intertropical convergence zone. *Nature*, **513**, 45–53, doi:10.1038/nature13636.

Sobel, A. H., 2007: Simple models of ensemble-averaged tropical precipitation and surface wind, given the sea surface temperature. *The Global Circulation of the Atmosphere*, T. Schneider and A. H. Sobel, Eds., Princeton University Press, 219–251.

——, and J. D. Neelin, 2006: The boundary layer contribution to intertropical convergence zones in the quasi-equilibrium tropical circulation model framework. *Theor. Comput. Fluid Dyn.*, **20**, 323–350, doi:10.1007/s00162-006-0033-y.

Stephens, G. L., D. O'Brien, P. J. Webster, P. Pilewski, S. Kato, and J.-L. Li, 2015: The albedo of Earth. *Rev. Geophys.*, **53**, 141–163, doi:10.1002/2014RG000449.

Trenberth, K. E., and J. M. Caron, 2001: Estimates of meridional atmosphere and ocean heat transports. *J. Climate*, **14**, 3433–3443, doi:10.1175/1520-0442(2001)014<3433:EOMAAO>2.0.CO;2.

——, and D. P. Stepaniak, 2003: Covariability of components of poleward atmospheric energy transports on seasonal and interannual timescales. *J. Climate*, **16**, 3691–3705, doi:10.1175/1520-0442(2003)016<3691:COCOPA>2.0.CO;2.

——, and J. T. Fasullo, 2008: An observational estimate of inferred ocean energy divergence. *J. Phys. Oceanogr.*, **38**, 984–999, doi:10.1175/2007JPO3833.1.

Vannière, B., E. Guilyardi, T. Toniazzo, G. Madec, and S. Woolnough, 2014: A systematic approach to identify the

sources of tropical SST errors in coupled models using the adjustment of initialized experiments. *Climate Dyn.*, **43**, 2261–2282, doi:10.1007/s00382-014-2051-6.

Voigt, A., and T. A. Shaw, 2015: Circulation response to warming shaped by radiative changes of clouds and water vapour. *Nat. Geosci.*, **8**, 102–106, doi:10.1038/ngeo2345.

Waliser, D. E., and R. C. J. Somerville, 1994: Preferred latitudes of the intertropical convergence zone. *J. Atmos. Sci.*, **51**, 1619–1639, doi:10.1175/1520-0469(1994)051<1619:PLOTIC>2.0.CO;2.

Walker, C. C., and T. Schneider, 2006: Eddy influences on Hadley circulations: Simulations with an idealized GCM. *J. Atmos. Sci.*, **63**, 3333–3350, doi:10.1175/JAS3821.1.

Xie, R., and Y. Yang, 2014: Revisiting the latitude fluctuations of the eastern Pacific ITCZ during the central Pacific El Niño. *Geophys. Res. Lett.*, **41**, 7770–7776, doi:10.1002/2014GL061857.

Yoshimori, M., and A. J. Broccoli, 2008: Equilibrium response of an atmosphere–mixed layer ocean model to different radiative forcing agents: Global and zonal mean response. *J. Climate*, **21**, 4399–4423, doi:10.1175/2008JCLI2172.1.

Zhang, C., 2001: Double ITCZs. *J. Geophys. Res.*, **106**, 11 785–11 792, doi:10.1029/2001JD900046.

Zhang, G. J., and H. Wang, 2006: Toward mitigating the double ITCZ problem in NCAR CCSM3. *Geophys. Res. Lett.*, **33**, L06709, doi:10.1029/2005GL025229.